

Comparison of ERS-2 SAR and Landsat TM imagery for monitoring agricultural crop and soil conditions

M. Susan Moran^{a,*}, Daniel C. Hymer^b, Jiaguo Qi^c, Yann Kerr^d

^aUSDA-ARS Southwest Watershed Research Center, 2000 East Allen Road, Tucson, AZ 85719, USA

^bNASA Goddard Space Flight Center, Greenbelt, MD, USA

^cMichigan State University, East Lansing, MI, USA

^dCentre d'Etudes Spatiales de la Biosphere (CESBIO), Toulouse, France

Received 21 September 1999; received in revised form 5 July 2000; accepted 17 July 2000

Abstract

Studies over the past 25 years have shown that measurements of surface reflectance and temperature (termed optical remote sensing) are useful for monitoring crop and soil conditions. Far less attention has been given to the use of radar imagery, even though synthetic aperture radar (SAR) systems have the advantages of cloud penetration, all-weather coverage, high spatial resolution, day/night acquisitions, and signal independence of the solar illumination angle. In this study, we obtained coincident optical and SAR images of an agricultural area to investigate the use of SAR imagery for farm management. The optical and SAR data were normalized to indices ranging from 0 to 1 based on the meteorological conditions and sun/sensor geometry for each date to allow temporal analysis. Using optical images to interpret the response of SAR backscatter (σ^0) to soil and plant conditions, we found that SAR σ^0 was sensitive to variations in field tillage, surface soil moisture, vegetation density, and plant litter. In an investigation of the relation between SAR σ^0 and soil surface roughness, the optical data were used for two purposes: (1) to filter the SAR images to eliminate fields with substantial vegetation cover and/or high surface soil moisture conditions, and (2) to evaluate the results of the investigation. For dry, bare soil fields, there was a significant correlation ($r^2=.67$) between normalized SAR σ^0 and near-infrared (NIR) reflectance, due to the sensitivity of both measurements to surface roughness. Recognizing the limitations of optical remote sensing data due to cloud interference and atmospheric attenuation, the findings of this study encourage further studies of SAR imagery for crop and soil assessment. © 2002 Elsevier Science Inc. All rights reserved.

1. Introduction

At this time, there are about 10 earth-observation satellites supporting optical sensors with the spatial, spectral, and temporal resolutions suitable for many farm management applications (Moran, Inoue, & Barnes, 1997). These optical sensors provide information in the reflective and thermal emissive portions of the electromagnetic spectrum. In a multitude of studies, this information has been used for such important farm applications as scheduling irrigations, predicting crop yields, and detecting certain plant diseases and insect infestations (see review by Hatfield & Pinter, 1993). Although optical remote sensing is a powerful farm management tool, there

are some serious limitations that have restricted farm management applications. For example, acquisitions are limited to cloud-free sky conditions, the signal is attenuated by the atmosphere, and image interpretation is a complex function of the sun/sensor/target geometry. An alternative to the use of optical remote sensing for farm management is the use of radar backscattering data obtained from synthetic aperture radar (SAR) sensors. There are currently four SAR sensors aboard polar-orbiting satellites, and there are plans for at least two more in the near future.

SAR sensors measure the spatial distribution of surface reflectivity in the microwave spectrum. The radar transmits a pulse and then measures the time delay and strength of the reflected echo (i.e., phase and amplitude measurements), where the ratio of scattered and incident microwave energy is termed the radar backscatter (σ^0). The scattering behavior of the SAR signal is governed by the dielectric properties of both soil and vegetation, and the geometric

* Corresponding author. Tel.: +1-520-670-6380X171; fax: +1-520-670-5550.

E-mail address: moran@tucson.ars.ag.gov (M.S. Moran).

configuration of the scattering elements (soil roughness, leaves, stalks, and fruit) with respect to the wavelength, direction, and polarization of the incident wave. SAR systems have the advantages of cloud penetration, all-weather coverage, high spatial resolution, day/night acquisitions, and signal independence of the solar illumination angle. These advantages allow SAR images to meet the rigid data requirements involved with farm management decisions. Furthermore, for agricultural applications, the inherent complexity of SAR interpretation is countered by the a priori information generally available from farm managers, such as cultivation practices, crop type, planting date, row direction, soil type, and topography (particularly with leveled or terraced fields).

The greatest weakness of SAR data for farm management is the poor understanding of the response of SAR σ^0 to agricultural soil and plant conditions. Research in the optical region has benefited from three factors: (1) the Large Area Crop Inventory Experiment (LACIE) and AgRISTARS programs, (2) availability of inexpensive, handheld optical sensors, and (3) access to reliable optical images from orbiting sensors, particularly Landsat Thematic Mapper (TM) and SPOT HRV. The LACIE and AgRISTARS programs defined the physics of relations between optical measurements and biophysical properties of crop canopies and soils (e.g., MacDonald & Hall, 1980). These pioneering programs established the potential of optical remote sensing for crop management, and inspired many studies of agricultural remote sensing. Subsequent studies advanced the science based on easy and often-inexpensive access to optical data obtained with handheld, airborne, or satellite-based sensors. SAR research has not had such advantages. First, there has not been a research effort of the magnitude of the LACIE and AgRISTARS Programs. Second, there are no commercially available, inexpensive, ground- or aircraft-based SAR sensors for intensive field experiments. Third, until 1990, there have been no SAR sensors aboard polar-orbiting satellites. Ultimately, these limitations make field studies of SAR applications for agricultural management very difficult at best.

Despite such difficulties, there have been multiple studies of SAR data for monitoring crop growth and development (e.g., Moran, Vidal, et al., 1997; Taconet et al., 1994; Ulaby, Allen, Eger, & Kanemasu, 1984). The best results have been obtained when SAR measurements are interpreted with reference to physical models that describe radar backscatter from crops and soils, such as the water cloud model (Attema & Ulaby, 1978), the Integrated Equation Model (IEM) (Fung, Li, & Chen, 1992; Oh, Sarabandi, & Ulaby, 1992), and the Michigan microwave canopy scattering (MIMICS) model (Ulaby, Sarabandi, McDonald, White, & Dobson, 1990). Such models have been inverted to determine important agricultural variables such as crop green leaf area index (GLAI) and surface soil moisture (e.g., Altese, Bolognani, Mancini, & Troch, 1996; Sano, Moran, Huete, & Miura, 1998).

However, the utility of the models has been limited by several factors. Empirical models, such as the water cloud model, require some model inputs that are unrelated to measurable physical quantities, and thus, must be calibrated based on model inversion with a large set of frequent SAR measurements. The IEM is only applicable to bare soils, and requires inputs that are difficult to measure at regional scales, such as surface roughness and surface soil moisture. The MIMICS model is a powerful tool for investigating the response of the SAR signal to plant and soil conditions, but like IEM, it is difficult to apply on a regional scale due to the requirement for multiple on-site measurements of soil and plant conditions. To avoid problems associated with measuring model inputs, crop growth and water balance models have been used to calculate the driving variables for the scattering models, such as the amount of water in the canopy and in the soil surface (e.g., Bouman, van Kraalingen, Stol, & van Leeuwen, 1999). The latter approach has some potential for agricultural application, but it requires a multitude of model inputs and the overall accuracy is dependent upon the accuracies of the three models.

This complexity and uncertainty of modeling approaches have spurred interest in the use of SAR/optical data synergy to combine the strengths of optical and SAR remote sensing to improve our ability to monitor agricultural resources. In the study presented here, we attempted to capitalize on the understanding of the response of the optical data to plant/soil conditions in order to interpret SAR images of an agricultural region. For four dates in 1995 through 1997, we acquired pairs of images from the Landsat TM sensor and the ERS-2 SAR sensor (Table 1) covering the University of Arizona Maricopa Agricultural Center (MAC) in central Arizona. TM measurements of multispectral reflectance (ρ) and temperature (T_s) measurements were used to interpret the ERS-2 C-band SAR backscatter (σ^0). In particular, we focused on the determination of within-field variations in

- soil roughness (related to tillage, subsidence, and erosion);

Table 1
Optical and radar sensor specifications for sensors used in the ASOS

Sensor	Spectral bands	Other specifications
Landsat-5 TM	Blue: 0.45–0.52 μm	Spatial resolution: 30 m (visible, NIR, SWIR) 120 m (thermal IR) Overpass time: ~ 10:30 am MST
	Green: 0.52–0.60 μm	
	Red: 0.63–0.69 μm	
	NIR: 0.76–0.90 μm	
	SWIR: 1.55–1.75 μm	
	SWIR: 2.08–2.35 μm	
	Thermal: 10.4–12.5 μm	
ERS-2 SAR	C band: 5.3 Ghz	4-looks format from ESA Spatial resolution: 25 m Pixel spacing: 12.5 m Incidence angle: 23°
	Polarization: VV	

- vegetation density (related to seeding, crop vigor, and pest infestations);
- surface soil moisture condition (related to monitoring irrigation efficacy and soil texture); and
- plant litter (related to erosion control).

Based on the complementary responses of optical and SAR signals to such soil/plant conditions, the sensitivity of SAR backscatter to surface roughness conditions was studied using a combined analysis of SAR and optical images. This work consisted of four processing steps. First, the spectral data were normalized to indices ranging from 0 to 1 based on the meteorological conditions and sun/sensor geometry for each date. Second, normalized surface reflectances in the red and near-infrared (NIR) reflectance wavelengths were used to discriminate vegetated and non-vegetated targets. Third, for nonvegetated targets, the normalized surface temperature was used to discriminate soil surfaces that were wet from those that were dry. Finally, for all nonvegetated, dry soil targets, the normalized SAR backscatter was related to the surface soil roughness based on a comparison with normalized NIR reflectance. This four-step approach is an example of the general idea that combining optical and SAR images will allow investigations that would not otherwise be possible with either image alone.

2. Background and theory

In the reflective region of the optical spectrum, discrimination of crop growth and plant status is generally accomplished by assessing the reflectance of red and NIR reflectance (ρ_{Red} and ρ_{NIR} , respectively) of the plant canopy. Simply put, plants absorb red radiation and scatter NIR radiation resulting in a large difference between ρ_{NIR} and ρ_{Red} ; in contrast, for bare soil, $\rho_{\text{NIR}} \approx \rho_{\text{Red}}$. This difference between plant and soil reflectances is often enhanced by computing a ratio of visible and NIR reflectances, termed a vegetation index (VI). A commonly used VI is the soil adjusted vegetation index

$$\text{SAVI} = (\rho_{\text{NIR}} - \rho_{\text{Red}}) / (\rho_{\text{NIR}} + \rho_{\text{Red}} + L)(1 + L), \quad (1)$$

where L is a unitless constant assumed to be 0.5 for a wide variety of leaf area index values (Huete, 1988). SAVI has been found to be sensitive to such vegetation parameters as GLAI, fraction absorbed photosynthetically active radiation, and percent of the ground surface covered by green vegetation (Jackson & Huete, 1991).

In the thermal region, remotely sensed measurements of soil and foliage temperature have been linked to soil moisture content, plant water stress, and plant transpiration rate (e.g., Norman, Divakarla, & Goel, 1995). The sensitivity of surface temperature to plant and soil moisture conditions is related primarily to the heat loss associated with evaporation and transpiration. As such, the thermal signal is related to the percentage of the site covered by green

vegetation and the water status of the vegetation and soil (i.e., EvapoTranspiration or ET).

In the microwave region, specifically the C-band SAR wavelength ($\lambda=6$ cm), it is generally assumed that σ° is directly related to surface roughness, soil moisture, and vegetation density. This can be expressed by the water cloud model, in which the power backscattered by the whole canopy σ° is the sum of the contribution of the vegetation σ_v° , and that of the underlying soil σ_s° . The latter is attenuated by the vegetation layer as a function of τ^2 , the two-way attenuation through the canopy. Thus,

$$\sigma^\circ = \sigma_v^\circ + \tau^2 \sigma_s^\circ, \quad (2)$$

where τ^2 is a function of GLAI, σ_v° is a function of τ^2 and GLAI, and σ_s° is a function of volumetric soil moisture content (h_v) and surface roughness (Prevot, Champion, & Guyot, 1993; Ulaby et al., 1984).

It is apparent from this short discussion that there is a relation between both the optical and SAR sensitivities to variations in soil surface roughness, vegetation density, and soil moisture (Table 2). Theoretically, as the surface roughness increases, σ° increases due to increased SAR scattering, ρ_{Red} and ρ_{NIR} decrease due to increased surface shadows, and T_s and SAVI remain relatively unchanged (though slight changes in both could be expected with increased surface shadows). As crop cover decreases, σ° generally increases due to an increase in τ^2 and a decrease in the attenuation of the soil backscatter (note that when $\sigma_v^\circ \gg \sigma_s^\circ$, it is possible for σ° to decrease with decreasing vegetation). Associated with decreases in crop cover, T_s increases due to decreased transpiration rate and increased radiation from the soil surface, ρ_{Red} increases due to decreased leaf chlorophyll, ρ_{NIR} decreases due to decreased leaf scattering, and the SAVI decreases dramatically. As surface soil moisture increases, σ° increases due to a change in the soil dielectric constant, T_s decreases due to increased evaporation rate, ρ_{Red} and ρ_{NIR} decrease due to water absorption, and the SAVI remains relatively unchanged. As bright, dry plant litter increases, σ° increases due to an increase in the underlying soil moisture, T_s and SAVI remain relatively unchanged, and ρ_{Red} and ρ_{NIR} both increase because litter is more reflective than the soil background.

Table 2

Theoretical response of optical and SAR measurements to changes in plant/soil condition, where \uparrow indicates an increase, \downarrow indicates a decrease, and $-$ indicates no substantial change

Change in plant/soil condition	σ°	T_s	ρ_{Red}	ρ_{NIR}	SAVI
Increase in surface roughness	\uparrow	$-$	\downarrow	\downarrow	$-$
Decrease in green vegetation biomass	\uparrow	\uparrow	\uparrow	\downarrow	\downarrow
Increase in surface soil moisture content	\uparrow	\downarrow	\downarrow	\downarrow	$-$
Increase in plant litter	\uparrow	$-$	\uparrow	\uparrow	$-$

σ° is backscatter, T_s is surface temperature, ρ_{Red} and ρ_{NIR} are surface reflectance in the Red and NIR spectrum, and SAVI is the soil adjusted vegetation index.

3. Experiment

The site of the Agricultural SAR/Optical Study (ASOS) was the University of Arizona MAC. MAC is a 770 ha research and demonstration farm located about 48 km south of Phoenix. The demonstration farm is composed of large fields (up to 0.27×1.6 km) in which alfalfa is grown year-round, cotton is grown during the summer, and wheat is grown during the winter. A data management system is in place to archive planting, harvesting, and tillage information, and the times and amounts of water, herbicide, and pesticide applications. Since the predominant irrigation method for the MAC demonstration farm is flooding, each field is dissected into level-basin “borders.”

ASOS was conducted in two parts. A retrospective study was conducted based on existing images in the European Space Agency (ESA) and EROS Data Center (EDC) archives. These images from 1995 and 1996 were ordered with the intent of determining field soil moisture, vegetation cover, tillage, and plant litter conditions based on the response of the optical and SAR signals, and validating these determinations with the field notes archived by the MAC Farm Manager. A second study was conducted in which we ordered TM/SAR image pairs for three dates (May, June, and July) in 1997. During all three overpasses, we arranged for one field to be flood-irrigated such that a large portion of the field was saturated, and, for contrast, a large portion was completely dry. A kenaf crop was planted in May, and by the June overpass dates, the GLAI was 0.3; by the July overpass, the GLAI was 1.5. We also monitored vegetation and soil moisture conditions in two fields of alfalfa at various growth stages with a variety of soil moisture conditions.

During each TM/SAR overpass in 1997, we made ~ 50 gravimetric measurements of soil moisture content to 5 cm depth in the dry and wet portions of the fallow field and in the two alfalfa fields. These were converted to volumetric soil moisture using estimates of field bulk density. We also measured GLAI in situ at multiple locations using a LICOR LAI2000 plant canopy analyzer.

The SAR raw data were averaged to one value for each field border (a minimum of 100 pixels) to minimize the speckle effect, and the mean was converted to values of σ^0 according to Moran, Vidal, et al. (1997). The TM data were also averaged to one value for each field border, and the means were converted to values of apparent reflectance and radiometric temperature according to Markham and Barker (1986) and Moran et al. (1995). The term “apparent reflectance” refers to reflectance factors derived from satellite images that have not been corrected for atmospheric effects. Considering that the TM data were acquired on days with clear, dry atmospheric conditions, the difference between apparent and surface reflectance in the red and NIR wavelengths should be minimal (Turner, Malila, Nelapka, & Thompson, 1975). Similarly, the radiometric temperature (T_r) measured by the TM sensor has been found to be within $1\text{--}2^\circ\text{C}$ of surface radiometric temperature for

days with clear, dry atmospheric conditions in central Arizona (Moran, 1990). T_r measured by the TM sensor was converted to surface kinetic temperature (T_s) based on measurements of surface emissivity (ϵ) using the relation $T_s = (T_r^4/\epsilon)^{1/4}$, where $\epsilon = 0.98$ for dense alfalfa, $\epsilon = 0.95$ for rough bare soil and recently harvested alfalfa, and $\epsilon = 0.89$ for laser-leveled bare soil (Reginato & Jackson, 1988).

Because there were few TM/SAR pairs available in the ESA and EDC archives, we were only able to obtain images for November and December 1995 and December 1996 (Table 3). During this time of year, there was very little farm activity, and the only crops were alfalfa and emergent wheat. Though we ordered the ERS-2 SAR and Landsat TM images for May, June, and July 1997, we only received one SAR/TM image pair (May 1997; Fig. 1). The reason for the failure to obtain the images as ordered is still unknown; however, such acquisition failure is not uncommon for satellite-based sensors, as reported by Moran (1994).

4. Approach

There are two approaches to SAR/optical data interpretation that are unique to this study and deserve further explanation here. One is the process of data normalization that allowed us to compare optical and SAR spectral measurements over time and space with common units, and the second is the approach for retrieval of soil surface roughness from SAR σ^0 using the four-step procedure mentioned briefly in the Introduction.

4.1. Data normalization

To monitor plant and soil variations either within a field or between images, we defined a set of normalized indices that allowed values of σ^0 , T_s , ρ_{Red} , ρ_{NIR} , and SAVI to be compared over space and time in values normalized to a range from 0 to 1. These indices allowed easy assessment of the optical and SAR responses to changes in plant/soil condition summarized in Table 2. Data from each image were converted to a normalized value as

Table 3
ERS-2 SAR and Landsat TM scenes ordered for the 1995–1997 ASOS

ERS-2 SAR	Landsat-5 TM	Notes
6 Nov. 1995	8 Nov. 1995	Wheat planted; cotton harvested; several disked fields; no irrigations
11 Dec. 1995	10 Dec. 1995	
30 Dec. 1996	28 Dec. 1996	
19 May 1997	21 May 1997	Soil moisture study with bare soil conditions in Field 3
23 June 1997	22 June 1997	Soil moisture study with kenaf GLAI=0.3 in Field 3 (SAR scene not acquired by ESA)
10 July 1997	9 July 1997	Soil moisture study with kenaf GLAI=1.5 in Field 3 (Neither the SAR nor TM scene was acquired)

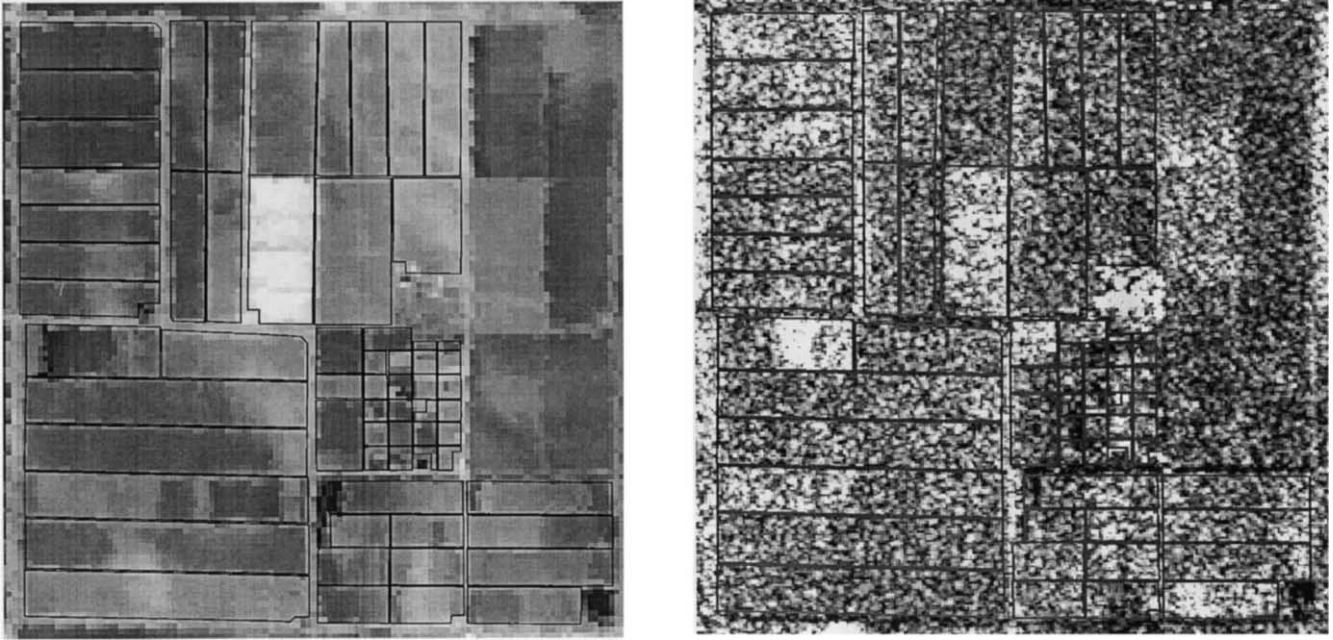


Fig. 1. Images of Landsat TM reflectance (left) and ERS-2 SAR backscatter (right) covering MAC acquired on 21 May and 19 May 1997, respectively. The vector overlay designates the MAC fields, and the total area covers 770 ha.

$$\sigma_N^{\circ} = (\sigma_A^{\circ} - \sigma_M^{\circ}) / (\sigma_X^{\circ} - \sigma_M^{\circ}), \quad (3)$$

$$T_{sN} = (T_{sA} - T_{sM}) / (T_{sX} - T_{sM}), \quad (4)$$

$$\rho_{\text{Red},N} = (\rho_{\text{Red},A} - \rho_{\text{Red},M}) / (\rho_{\text{Red},X} - \rho_{\text{Red},M}), \quad (5)$$

$$\rho_{\text{NIR},N} = (\rho_{\text{NIR},A} - \rho_{\text{NIR},M}) / (\rho_{\text{NIR},X} - \rho_{\text{NIR},M}), \quad (6)$$

$$\text{SAVI}_N = (\text{SAVI}_A - \text{SAVI}_M) / (\text{SAVI}_X - \text{SAVI}_M), \quad (7)$$

where the subscript N indicates that the value has been normalized, subscript A refers to the actual value, and subscripts X and M refer to the maximum and minimum values for that date and time (as described below). For change detection, e.g., within-field analysis, normalized difference (Δ_N) indices were computed, where

$$\Delta_N \sigma^{\circ} = \sigma_{N,1}^{\circ} - \sigma_{N,2}^{\circ} = (\sigma_1^{\circ} - \sigma_2^{\circ}) / (\sigma_X^{\circ} - \sigma_M^{\circ}), \quad (8)$$

$$\Delta_N T_s = T_{s,N,1} - T_{s,N,2} = (T_{s1} - T_{s2}) / (T_{sX} - T_{sM}), \quad (9)$$

$$\begin{aligned} \Delta_N \rho_{\text{Red}} &= \rho_{\text{Red},N,1} - \rho_{\text{Red},N,2} \\ &= (\rho_{\text{Red}1} - \rho_{\text{Red}2}) / (\rho_{\text{Red}X} - \rho_{\text{Red}M}), \end{aligned} \quad (10)$$

$$\begin{aligned} \Delta_N \rho_{\text{NIR}} &= \rho_{\text{NIR},N,1} - \rho_{\text{NIR},N,2} \\ &= (\rho_{\text{NIR}1} - \rho_{\text{NIR}2}) / (\rho_{\text{NIR}X} - \rho_{\text{NIR}M}), \end{aligned} \quad (11)$$

$$\begin{aligned} \Delta_N \text{SAVI} &= \text{SAVI}_{N,1} - \text{SAVI}_{N,2} \\ &= (\text{SAVI}_1 - \text{SAVI}_2) / (\text{SAVI}_X - \text{SAVI}_M), \end{aligned} \quad (12)$$

where the subscripts 1 and 2 refer to two locations within the field and Δ_N values range from -1 to 1 .

The minimum and maximum values of σ° , T_s , ρ_{Red} , ρ_{NIR} , and SAVI were computed as follows. For σ° , we assumed that the ERS-2 sensor calibration was accurate and that σ° would vary only with surface conditions. Consequently, it was possible to determine σ_X° and σ_M° based solely on the data within the four images; that is, σ_X° was equal to the maximum σ° for the agricultural fields in the four images, and similarly, σ_M° was equal to the minimum σ° . This resulted in $\sigma_M^{\circ} = -16$ and $\sigma_X^{\circ} = +5$. A similar approach was used for SAVI_X and SAVI_M . Considering that the SAVI has already been normalized for soil differences (Eq. (1)) and that SAVI varies minimally with differences in solar zenith angle (Pinter, Jackson, & Moran, 1990), we set SAVI_X equal to the maximum SAVI for the agricultural fields in the four images, and SAVI_M equal to the minimum SAVI. Thus, $\text{SAVI}_X = 0.7$ and $\text{SAVI}_M = 0.0$.

Surface reflectance is highly dependent upon solar zenith angle (θ_z) due to variations in the amount of shadow on the surface (Jacquemoud, Baret, & Hanocq, 1992). This relation between ρ and θ_z can be approximated as a function of $\cos(\theta_z)$ for many vegetated and rough soil surfaces (Dymond & Qi, 1997). To compute $\rho_{\text{Red},X}$, $\rho_{\text{Red},M}$, $\rho_{\text{NIR},X}$, and $\rho_{\text{NIR},M}$, we first estimated a maximum and minimum reflectance that

would be measured from shadowless bright and dark soil/plant surfaces, respectively. These minimum and maximum values were estimated to be 0.02 and 0.8 for the red spectral band, and 0.1 and 0.9 for the NIR spectral band. These “extreme” values were multiplied by $\cos(\theta_z)$ for each date, resulting in the following values for each scene:

8 Nov. 1995	$\theta_z = 55.4$	$\rho_{\text{Red,X}} = 0.45$	$\rho_{\text{Red,M}} = 0.01$	$\rho_{\text{NIR,X}} = 0.51$	$\rho_{\text{NIR,M}} = 0.06$
10 Dec. 1995	$\theta_z = 61.9$	$\rho_{\text{Red,X}} = 0.38$	$\rho_{\text{Red,M}} = 0.01$	$\rho_{\text{NIR,X}} = 0.42$	$\rho_{\text{NIR,M}} = 0.05$
26 Nov. 1996	$\theta_z = 59.8$	$\rho_{\text{Red,X}} = 0.40$	$\rho_{\text{Red,M}} = 0.01$	$\rho_{\text{NIR,X}} = 0.45$	$\rho_{\text{NIR,M}} = 0.05$
21 May 1997	$\theta_z = 28.4$	$\rho_{\text{Red,X}} = 0.70$	$\rho_{\text{Red,M}} = 0.02$	$\rho_{\text{NIR,X}} = 0.79$	$\rho_{\text{NIR,M}} = 0.09$

The values of maximum and minimum T_s are a function of the meteorological conditions at the time and date of overpass based on the Penman–Monteith equation (Allen, 1986),

$$\lambda E_{\Gamma} = [\Delta(R_n - G) + \rho C_p(\text{VPD})/r_a]/[\Delta + \gamma^*], \quad (13)$$

where λE_{Γ} is the latent heat flux (W m^{-2}), Δ is the slope of the saturation vapor pressure–temperature curve (kPa C^{-1}), R_n is the net radiation flux at the surface (W m^{-2}), G is the sensible heat flux conducted to the soil (W m^{-2}), ρ is air density (kg m^{-3}), C_p is specific heat at constant pressure ($\text{kJ kg}^{-1} \text{C}^{-1}$), VPD is vapor pressure deficit (kPa), and the aerodynamic resistance, r_a (s m^{-1}) is (Eq. (14))

$$r_a = \{[\ln((z - d_o)/z_{om}) + \ln(z_{om}/z_{oh}) - \Phi_h] \\ \times [\ln((z - d_o)/z_{om}) - \Phi_m]\}/k^2 u, \quad (14)$$

and u is wind speed (m s^{-1}), z is the height above the surface at which u is measured (m), d_o is the displacement height (m), z_{om} and z_{oh} are the roughness lengths for momentum and heat (m), respectively, Φ_h and Φ_m are the stability corrections for heat and momentum, respectively, and k is von Karman’s constant (≈ 0.4). The value of γ^* (kPa C^{-1}) in Eq. (13) is a function of r_a and the canopy resistance to vapor transport (r_c , s m^{-1}), where $\gamma^* = \gamma(1 + r_c/r_a)$.

Jackson, Idso, Reginato, and Pinter (1981) derived an equation to compute vegetation temperature based on Eq. (13) and a measure of air temperature. Moran, Clarke, Inoue, and Vidal (1994) showed that this equation could be used to compute the minimum and maximum temperatures ($T_{s,X}$ and $T_{s,M}$) of a bare soil surface. For saturated bare soil, where $r_c = 0$ (the case of a free water surface),

$$T_{s,M} = T_a + [r_a(R_n - G)/\rho C_p][\gamma/(\Delta + \gamma)] \\ - [\text{VPD}/(\Delta + \gamma)], \quad (15)$$

and for dry bare soil, where $r_c = \infty$ (analogous to complete stomatal closure),

$$T_{s,X} = T_a + [r_a(R_n - G)/\rho C_p]. \quad (16)$$

Based on on-site meteorological measurements and the approaches described by Moran et al. (1994), values of $T_{s,X}$

and $T_{s,M}$ were derived for each of the four Landsat images using Eqs. (15) and (16) with the following results:

8 Nov. 1995	$T_{s,X} = 25.7$	$T_{s,M} = 13.7$
10 Dec. 1995	$T_{s,X} = 21.6$	$T_{s,M} = 11.9$
26 Nov. 1996	$T_{s,X} = 25.0$	$T_{s,M} = 13.5$
21 May 1997	$T_{s,X} = 47.4$	$T_{s,M} = 21.6$

The normalization of the optical data reduced the influences of variations in meteorological condition and sun/sensor geometry for each date to allow temporal analysis. The normalization of the SAR data, as performed in this study, converted the data into units ranging from 0 to 1, but was not a required transformation for this temporal analysis.

4.2. Retrieval of soil surface roughness from SAR backscatter

A simple approach was used to retrieve soil surface roughness from measured SAR backscatter through a series of steps in which the SAR data were filtered based on concurrent measurements in optical wavelengths. This approach was based on the premise that the dominant influences on SAR backscatter of a given wavelength and polarization are (1) surface soil moisture, (2) vegetation density, and (3) surface roughness (Eq. (2)). For dry surfaces devoid of vegetation, the dominant influence on SAR backscatter was surface roughness. According to Table 2, the only surface condition that substantially affected SAVI was a change in green vegetation biomass. Thus, the SAVI was used to discriminate vegetated from nonvegetation targets. Again according to Table 2, for nonvegetated surfaces, the only surface condition that substantially affected surface temperature was a change in surface soil moisture condition. Thus, T_s was used to discriminate bare soils with wet and dry surface conditions. Using SAVI and T_s as image filters, it was possible to identify all the pixels in the SAR image associated with dry, bare soil. Then, according to Eq. (2), the dominant influence on the magnitude of SAR backscatter was surface roughness.

Based on the averages of spectral information retrieved from each of 260 field borders for all eight Landsat TM and ERS-2 SAR scenes, the values of $T_{s,N}$ and SAVI_N were used to eliminate field borders that were vegetated or had wet surface soil conditions. Data from all borders with $\text{SAVI}_N > 0.1$ and $T_{s,N} < 0.35$ were removed from the data

set. With these thresholds, the remaining data were from field borders characterized by dry, bare soils with a variety of surface roughness conditions. Based on the assumption that $\rho_{NIR,N}$ of dry, bare soil surfaces is dominantly influenced by shadowing from roughness elements (Jacquemoud et al., 1992), a scattergram of σ_N° and $\rho_{NIR,N}$ produced a strong negative relation for this filtered data set.

5. Results and discussion

Results from the ASOS experiments are presented in three sections. First, results from the soil moisture and vegetation study in 1997 are presented; second, Δ_N indices derived from Eqs. (8)–(12) were used to support the general trends presented in Table 2; and third, normalized spectral values (Eqs. (3)–(7)) from all four images were combined to assess the suitability of SAR imagery to map farm-scale soil roughness for agricultural resources management.

5.1. ASOS soil moisture experiment 1997

The study conducted in May 1997 was designed to investigate the sensitivity of SAR and optical data to differing soil moisture conditions. A large portion of a fallow field was flood irrigated during the ERS-2 and Landsat overpasses, and another portion was left dry. Measurements of SAR σ° , T_s , ρ_{Red} , ρ_{NIR} , and SAVI were extracted from the SAR and TM scenes for the very wet and very dry portions of the field. These data confirmed the theoretical response of SAR and optical data to changes in surface soil moisture conditions (Fig. 2). That is, for a soil moisture increase of 35%, the SAR σ° increased by nearly 8 dB, T_s decreased by 8°C, ρ_{Red} and ρ_{NIR} decreased by 0.07 each, and SAVI remained nearly constant with an increase

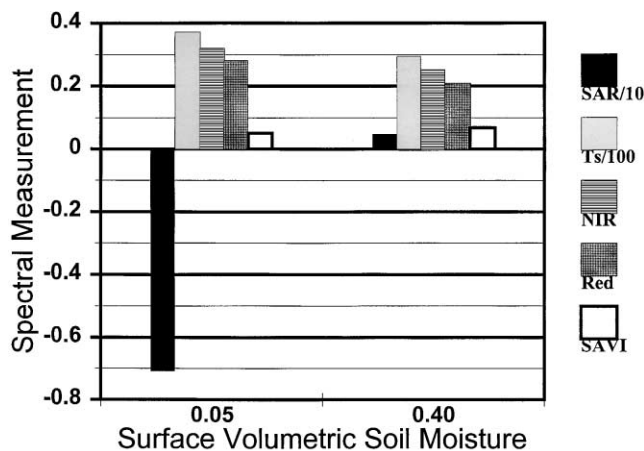


Fig. 2. Measurements of SAR backscatter (σ), surface temperature, NIR and Red reflectance and SAVI in two sections of a fallow field with differing soil moisture conditions. For purposes of graphic clarity, the SAR σ° values were divided by 10 and the T_s values were divided by 100.

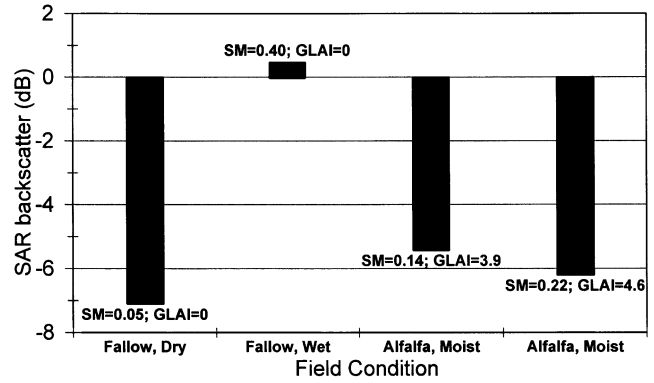


Fig. 3. A comparison of the sensitivity of SAR backscatter to soil moisture and vegetation density conditions for a fallow field and an alfalfa field. In the figure, the bars are labeled with measurements of volumetric soil moisture (SM) and GLAI.

of 0.02. These results demonstrated the substantial changes in σ° , T_s , ρ_{Red} , and ρ_{NIR} due to soil moisture variations for bare soil conditions.

For crops with $GLAI > 1.0$, the sensitivity of the SAR σ° to surface soil moisture content is substantially decreased (Moran, Vidal, Troufleau, Inoue, & Mitchell, 1998). For the two MAC alfalfa fields with $GLAI \sim 4.0$, the σ° was completely insensitive to the difference in soil moisture in the two fields, and instead, responded to the differences in GLAI (Fig. 3). That is, the σ° increased with decreasing GLAI. According to Eq. (2), the transmittance through the dense alfalfa canopy (τ^2) was low, and thus the SAR σ° was dominated by the backscatter signal from the vegetation (σ_v°). This is discouraging for the use of SAR images for irrigation scheduling purposes late in the growing season. However, information about surface soil moisture condi-

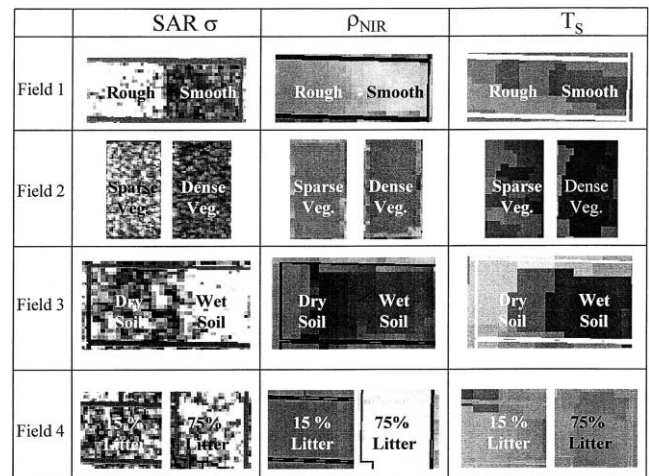


Fig. 4. Extracts of SAR and optical data for the four study fields, illustrating the differences in spectral response in SAR backscatter, NIR reflectance, and radiometric surface temperature to variations in field tillage, vegetation density, surface soil moisture, and plant litter.

tions obtained early in the growing season is still useful for monitoring irrigation efficacy, mapping precipitation events, and determining soil texture.

5.2. Δ_N indices for within-field change detection

We selected all MAC fields in the four 1995–1997 images that had a record of distinctive within-field differences in tillage, soil moisture, vegetation density, and plant litter. Since results were similar for fields of similar surface conditions, four fields were selected as examples for illustration in this section. According to field notes and on-site observations, Field 1 was fallow, but part of the field had been laser leveled and part was still rough due to cultivation; Field 2 was planted with alfalfa, but half of the field had been recently harvested; Field 3 was also fallow, but part of the field had been flood irrigated; and Field 4 had two sections with different amounts of the surface covered with dry plant litter.

All four fields (numbered 1–4 for reference herein) had a notable increase in the SAR σ° ($\Delta_N\sigma^\circ \sim 0.2$) from one end of the field to the other (Figs. 4 and 5). The increase in $\Delta_N\sigma^\circ$ in Field 1 was due to the increased scattering of the SAR signal due to soil roughness. In Field 2, the increase in $\Delta_N\sigma^\circ$ resulted from a decrease in the alfalfa crop density due to a recent harvest, resulting in a larger τ^2 value in Eq. (2). In Field 3, $\Delta_N\sigma^\circ$ increased due to the change in soil moisture and the sensitivity of the SAR signal to the dielectric constant of the surface. The dielectric constant of water is about 80 (in the C-band wavelength) and that of dry vegetation or soil is about 2–3. In Field 4, $\Delta_N\sigma^\circ$ apparently increased due to an increase in dry crop litter cover from 15% to 75%.

The visual and quantitative assessment presented in Figs. 4 and 5 showed that the response of the optical data to the three different field conditions corresponded well with the

theoretical hypotheses presented in Table 2. In Field 1, as the soil roughness increased, $\Delta_N\rho_{NIR}$ and $\Delta_N\rho_{Red}$ decreased by 0.2 due to increased surface shadows, and $\Delta_N T_s$ and $\Delta_N SAVI$ remained near zero for the two roughnesses. In Field 2, as the vegetation decreased due to harvest, $\Delta_N T_s$ increased by about 0.2 due to the decrease in transpiration, $\Delta_N\rho_{NIR}$ decreased by 0.5 and $\Delta_N\rho_{Red}$ increased by 0.4 due to the decrease in leaf area and photosynthetic activity, causing a decrease in $\Delta_N SAVI$ of 0.62. In Field 3, as the soil moisture increased, $\Delta_N T_s$ decreased by about 0.5 due to evaporative cooling, $\Delta_N\rho_{NIR}$ and $\Delta_N\rho_{Red}$ decreased by approximately 0.1 due to water absorption, and $\Delta_N SAVI$ remained near zero. In Field 4, as the percentage of the surface covered with dry plant litter increased, $\Delta_N\rho_{NIR}$ and $\Delta_N\rho_{Red}$ increased by approximately 0.4 because the litter reflectance was higher than the soil reflectance in both bands.

Based on data for fields not illustrated in Figs. 4 and 5, we found that the optical data were also useful for discriminating “mixes” of effects of roughness, vegetation, and soil moisture. For example, in the SAR image acquired in November 1995, two adjacent fields of alfalfa showed no difference in SAR σ° ($\Delta_N\sigma^\circ \sim 0$), despite large negative values of $\Delta_N T_s$ and $\Delta_N SAVI$. Based on the optical response, we postulated that one of the fields had been recently harvested and had a low soil moisture content; the other was near 100% vegetation cover and had been recently irrigated. As a result, the high σ° associated with low crop cover was offset by the low σ° associated with high soil moisture content, and $\Delta_N\sigma^\circ \sim 0$.

Overall, the Δ_N indices worked well to discriminate the causal relation between surface conditions and SAR σ° . Though results for only four fields are illustrated here, similar results for several more fields showed that this method has potential for interpretation of SAR imagery with coincident optical imagery. These results also illustrated the sensitivity of Landsat TM and ERS-2 SAR imagery to differences in tillage, surface soil moisture, vegetation density, and dry crop litter.

5.3. Retrieval of farm-scale soil roughness from SAR σ°

The approach for retrieval of soil surface roughness from SAR σ° , described in the previous section, is based on the premise that σ° is directly related to the soil surface roughness of dry bare soils. Further, this relation can be qualitatively assessed by the negative correlation between σ° and $\rho_{NIR,N}$ due to theoretically inverse sensitivities to surface roughness conditions. All available data from the four TM/ERS-2 image pairs were combined for this study; this data set included nine MAC fields with three to eight borders in each field with measurements on four dates, resulting in 260 points total. Without any data normalization or filtering, there was no discernable relation between σ° and ρ_{NIR} (Fig. 6A). The first step in the approach was to normalize the values of σ° , T_s , ρ_{Red} , ρ_{NIR} , and SAVI, as described in the previous section. This normalization allowed the measurements from the four dates

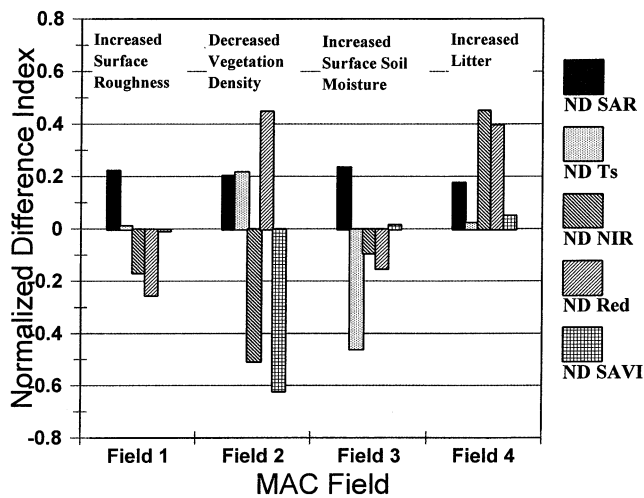


Fig. 5. The response of Δ_N indices (Eqs. (8–12) to variations in field roughness, vegetation density, and surface soil moisture. The five legend captions refer to $\Delta_N\sigma^\circ$, $\Delta_N T_s$, $\Delta_N\rho_{Red}$, $\Delta_N\rho_{NIR}$, and $\Delta_N SAVI$, respectively.

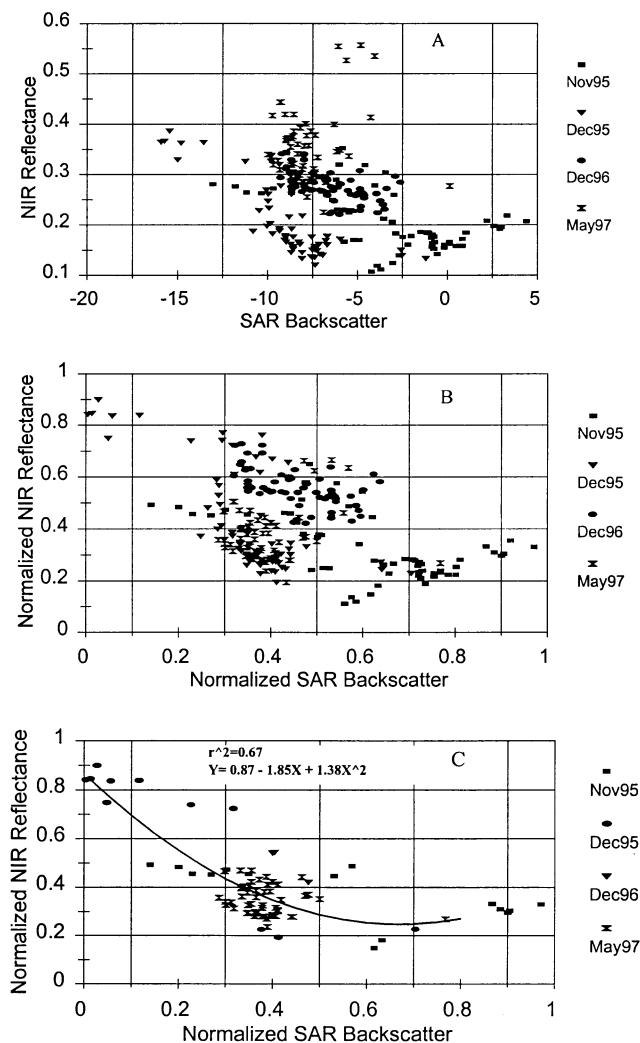


Fig. 6. Relations between (A) SAR backscatter and NIR reflectance and (B) normalized SAR backscatter and normalized NIR reflectance for all MAC fields on four dates. Relation between (C) normalized SAR backscatter and normalized NIR reflectance for dry, bare soil fields only.

to be compared regardless of variations in solar zenith angle or meteorological conditions at the time of image acquisition. There appeared to be a weak negative relation between σ_N° and $\rho_{\text{NIR},N}$ that was complicated by the interactions of surfaces with differing soil moistures, roughnesses, and vegetation densities (Fig. 6B). A subset of image pixels with $\text{SAVI}_N < 0.1$ and $T_{s,N} > 0.35$ (assumed to be associated with dry, bare soils) was extracted; this subset included 3–5 fields per each of the four dates with three to eight borders in each field, resulting in 84 points total. For this subset, there was a statistically significant, second-order, negative relation between σ_N° and $\rho_{\text{NIR},N}$ (Fig. 6C).

The shape and scatter in the relation between σ_N° and $\rho_{\text{NIR},N}$ for dry, bare soils was explained in several ways. First, the premise of this investigation was that σ_N° was related to surface roughness for dry, bare soils. Since measurements of surface roughness for each field were

not available, σ_N° was compared with $\rho_{\text{NIR},N}$ based on the assumption that $\rho_{\text{NIR},N}$ was equally sensitive to surface roughness. This may not be a robust assumption because:

1) the “roughness” measured by σ_N° is based on the geometry of the radar beam and the surface (where a field of east/west oriented furrows would not have the same apparent roughness as a field with north/south furrows), whereas the roughness measured by $\rho_{\text{NIR},N}$ is based on the geometry of the solar beam and the surface;

2) the curvilinear relation between σ_N° and $\rho_{\text{NIR},N}$ suggests that the values of $\rho_{\text{NIR},N}$ reach a threshold, despite apparent further increases in roughness measured by σ_N° ; and

3) $\rho_{\text{NIR},N}$ is influenced not only by surface roughness but also by the soil composition, resulting in variations in $\rho_{\text{NIR},N}$ that are independent of roughness.

Another source of scatter was likely due to changes in field conditions over the two- to three-day period between optical and SAR image acquisitions for each of the four image pairs (Table 3). Furthermore, with this filtering approach, there were no adjustments made for the unknown variations in plant litter among the targets. Finally, the thermal data used to filter the data for soil moisture condition is only sensitive to the top 1 mm of the soil, whereas SAR measurements can penetrate the surface to measure soil moisture in the top 1–5 cm, depending upon soil moisture condition. Though this investigation resulted in a significant relation between σ_N° and $\rho_{\text{NIR},N}$, additional validation experiments are warranted.

6. Concluding remarks

The objective of this study was to investigate the utility of SAR images for farm management applications. These results showed that the SAR σ° was sensitive to differences in field roughness (related to tillage), vegetation density, surface soil moisture, and dry plant litter. Furthermore, we found that optical imagery obtained coincident with SAR imagery allowed a better understanding of the interactions of the SAR signal with soil and plant surfaces. Since it is oftentimes difficult to interpret a single-band SAR image over a diverse agricultural landscape, a coincident optical image provided surface information necessary to investigate SAR suitability for agricultural applications. An approach for normalization of optical and SAR data (converting values to a scale of 0 to 1) was proposed to allow comparison of optical and SAR spectral measurements over time and space with common units.

This study also demonstrated that combining optical and SAR images could allow analyses of SAR data that would not otherwise be possible with the SAR imagery alone. As an example of this concept, optical data were used to filter the SAR images to include only dry, bare soil fields to investigate the sensitivity of SAR σ° to soil surface roughness. The results were evaluated qualitatively by comparison of SAR σ° and NIR ρ (both theoretically

sensitive to surface roughness) for a variety of agricultural fields of different roughnesses. A significant negative correlation between normalized σ° and ρ_{NIR} values provided support for the hypothesis that σ° was useful in monitoring regional surface roughness conditions related to agricultural tillage, subsidence, and erosion. Such optical/SAR investigations help to identify the most promising approaches for application of SAR measurements for monitoring agricultural conditions. Recognizing the limitations of optical remote sensing data due to cloud interference and atmospheric attenuation, the findings of this study encourage further studies of SAR imagery for crop and soil assessment.

Acknowledgments

We would like to acknowledge valuable help from Wanmei Ni, Chandra Holifield, Ross Bryant, Robin Marsett, Michael Helfert, and Yann Nouvellon, and the cooperation of personnel at the University of Arizona Maricopa Agricultural Center (MAC). Financial support was provided by the NASA Landsat Science Team (NASA S-41396-F), NASA EOS IDS (NAGW-2425), and European Space Agency (ESA-AO2.F119).

References

- Allen, R. G. (1986). A Penman for all seasons. *Journal of Irrigation and Drainage Engineering*, *112*, 348–368.
- Altse, E., Bolognani, O., Mancini, M., & Troch, P. A. (1996). Retrieving soil moisture over bare soil from ERS 1 synthetic aperture radar data: sensitivity analysis based on a theoretical surface scattering model and field data. *Water Resources Research*, *32*, 653–661.
- Attema, E. P. W., & Ulaby, F. T. (1978). Vegetation modeled as a water cloud. *Radio Science*, *13*, 357–364.
- Bouman, B. A. M., van Kraalingen, D. W. G., Stol, W., van Leeuwen, H. J. C. (1999). An agroecological modeling approach to explain ERS SAR radar backscatter of agricultural crops. *Remote Sensing of Environment*, *67*, 137–146.
- Dymond, J. R., & Qi, J. (1997). Reflection of visible light from a dense vegetation canopy — a physical model. *Agricultural and Forest Meteorology*, *86*, 143–155.
- Fung, A. K., Li, Z., & Chen, K. S. (1992). Backscattering from a randomly rough dielectric surface. *IEEE Transactions on Geoscience and Remote Sensing*, *30*, 356–369.
- Hatfield, J. L., & Pinter, P. J. Jr. (1993). Remote sensing for crop protection. *Crop Protection*, *12*, 403–414.
- Huete, A. R. (1988). A soil-adjusted vegetation index (SAVI). *Remote Sensing of Environment*, *25*, 89–105.
- Jackson, R. D., & Huete, A. R. (1991). Interpreting vegetation indices. *Preventive Veterinary Medicine*, *11*, 185–200.
- Jackson, R. D., Idso, D. B., Reginato, R. J., & Pinter, P. J. Jr. (1981). Canopy temperature as a crop water stress indicator. *Water Resources Research*, *17*, 1133–1138.
- Jacquemoud, S., Baret, F., & Hanocq, J. F. (1992). Modeling spectral and bidirectional soil reflectance. *Remote Sensing of Environment*, *41*, 123–132.
- MacDonald, R. B., & Hall, F. G. (1980). Global crop forecasting. *Science*, *208*, 670–679.
- Markham, B. L., & Barker, J. L. (1986). Landsat MSS and TM post-calibration dynamic ranges, exoatmospheric reflectances and at-satellite temperatures. *EOSAT Landsat Technical Notes*, *1*, 3–8.
- Moran, M. S. (1990). *A satellite-based approach for evaluation of the spatial distribution of evapotranspiration from agricultural lands*. PhD Dissertation, Department of Soil and Water Science, Univ. of Ariz., Tempe, AZ, pp. 223.
- Moran, M. S. (1994). Irrigation management in Arizona using satellites and airplanes. *Irrigation Science*, *15*, 35–44.
- Moran, M. S., Clarke, T. R., Inoue, Y., & Vidal, A. (1994). Estimating crop water deficit using the relation between surface-air temperature and spectral vegetation index. *Remote Sensing of Environment*, *49*, 246–263.
- Moran, M. S., Inoue, Y., & Barnes, E. M. (1997). Opportunities and limitations for image-based remote sensing in precision crop management. *Remote Sensing of Environment*, *61*, 319–346.
- Moran, M. S., Jackson, R. D., Clarke, T. R., Qi, J., Cabot, F., Thome, K. J., & Markham, B. L. (1995). Reflectance factor retrieval from Landsat TM and SPOT HRV data for bright and dark targets. *Remote Sensing of Environment*, *52*, 218–230.
- Moran, M. S., Vidal, A., Troufleau, D., Inoue, Y., & Mitchell, T. A. (1998). Ku- and C-band SAR for discriminating agricultural crop and soil conditions. *IEEE Transactions on Geoscience and Remote Sensing*, *36*, 265–272.
- Moran, M. S., Vidal, A., Troufleau, D., Qi, J., Clarke, T. R., Pinter, P. J. Jr., Mitchell, T. A., Inoue, Y., & Neale, C. M. U. (1997). Combining multi-frequency microwave and optical data for farm management. *Remote Sensing of Environment*, *61*, 96–109.
- Norman, J. M., Divakarla, M., & Goel, N. S. (1995). Algorithms for extracting information from remote thermal-IR observations of the earth's surface. *Remote Sensing of Environment*, *51*, 157–168.
- Oh, Y., Sarabandi, K., & Ulaby, F. T. (1992). An empirical model and an inversion technique for radar scattering from bare soil surfaces. *IEEE Transactions on Geoscience and Remote Sensing*, *30*, 370–381.
- Pinter, P. J. Jr., Jackson, R. D., & Moran, M. S. (1990). Bidirectional reflectance factors of agricultural targets: a comparison of ground-, aircraft- and satellite-based observations. *Remote Sensing of Environment*, *32*, 215–228.
- Prevot, L., Champion, I., & Guyot, G. (1993). Estimating surface soil moisture and leaf area index of a wheat canopy using dual-frequency (C and X bands) scatterometer. *Remote Sensing of Environment*, *46*, 331–339.
- Reginato, R. J., & Jackson, R. D. (1988). *Emissivity measurements of soil and plant surfaces*. Chapter 9 in The MAC III Experiment Report, USDA-ARS U.S. Water Conservation Laboratory, Phoenix, AZ.
- Sano, E. E., Moran, M. S., Huete, A. R., & Miura, T. (1998). C- and multiangle Ku-band synthetic aperture radar data for bare soil moisture estimation in agricultural areas. *Remote Sensing of Environment*, *64*, 77–90.
- Taconet, O., Benallegue, M., Vidal-Madjar, D., Prevot, L., Dechambre, M., & Normand, M. (1994). Estimation of soil and crop parameters for wheat from airborne radar backscattering data in C and X bands. *Remote Sensing of Environment*, *50*, 287–294.
- Turner, R. E., Malila, W. A., Nelapka, R. F., & Thompson, F. J. (1975). Influence of the atmosphere on remotely sensed data. *Proceedings of SPIE*, *51*, 101–110.
- Ulaby, F. T., Allen, C. T., Eger, G. III, & Kanemasu, E. (1984). Relating the microwave backscattering coefficient to leaf area index. *Remote Sensing of Environment*, *14*, 113–133.
- Ulaby, F. T., Sarabandi, K., McDonald, K., White, M., & Dobson, M. C. (1990). Michigan microwave canopy scattering model. *International Journal of Remote Sensing*, *11*, 1223–1253.